JOURNAL OF MATERIALS SCIENCE 27 (1992) 1085–1100

Fracture resistance of a glass-fibre reinforced rubber-modified thermoplastic hybrid composite

S. V. NAIR, M. L. SHIAO
Department of Mechanical Engineering, University of Massachusetts, Amherst, MA 01002, USA

P. D. GARRETT
Monsanto Chemical Co., 730 Worcester Street, Springfield, MA 01151, USA

Toughening mechanisms in a hybrid amorphous thermoplastic composite containing both distributed rubber particles and rigid glass fibres have been investigated. Tensile properties were measured for a range of materials with varying rubber particle and glass-fibre contents, and different rubber particle sizes. Fracture toughness was characterized by separating the overall fracture into its initiation and propagation components. Deformation and fracture modes at crack tips were optically characterized *in situ* during loading. The results indicate that both initiation and propagation toughness are enhanced by rubber particle additions to the glass-fibre reinforced composite. Synergistic effects between glass fibres and rubber particles are identified: for example, glass fibres inhibit crazing at rubber particles, and rubber particles tend to promote crazing at fibre/matrix interfaces and also void initiation at fibre ends. Toughening mechanisms are discussed in the light of available models.

1. Introduction

Hybrid thermoplastic composites, involving more than one type of second-phase addition, have been successfully applied to improve the properties and cost effectiveness of thermoplastics [1–3]. Examples are additions of ductile particles combined with rigid fibres [4–9]; brittle particles [10]; or addition of different fibre types such as carbon and glass-fibre mixtures [11]. This paper reports on the fracture resistance and toughening mechanisms in a short-glass-fibre reinforced glassy thermoplastic composite containing fine rubber particle additions to the matrix.

The toughening strategy in glassy polymers using distributed rubber particles has long been recognized [12–16]. The fundamental toughening mechanisms are generally associated with localized deformations around the added rubber particles in the form of crazes and/or shear bands [17, 18] which also serve to dissipate additional energy in the crack-tip region. On the other hand, with short high-modulus fibre additions, toughening can result from crack deflection [19], fibre/matrix debonding, fibre bridging of cracks, and fibre pull-out effects [20, 21]. The toughening mechanisms under the combined presence of both rubber particles and fibre reinforcements have received limited attention. Interactive effects are suggested by previous studies [5–9]. For example, addition of glass fibres to styrene acrylonitrile (SAN) or polystyrene polymers increases the fracture resistance, whereas in the presence of rubber modification, as in acrylonitrile-butadiene-styrene (ABS), glass fibres appear to reduce toughness [9]. Similar results have been reported for a rubber-modified and glass-fibre reinforced semi-crystalline polyamide thermoplastic [5]. In addition, glass fibres have been reported to inhibit the toughening influence of rubber particles above some critical volume fraction [5, 8] consistent with other results in rubber-modified and fibre-reinforced epoxy systems [4]. This synergism between glass fibres and rubber particles is not well understood.

The strategy in this study has been to evaluate the toughness of a range of materials with varying glass-fibre and rubber-particle contents, as well as rubber particle sizes. Both the initiation and propagation components of toughness are measured because the mechanisms governing crack initiation and growth are in general different, and each component can contribute significantly to the overall toughness of the hybrid composites. Further, *in situ* examination during loading is used to study localized deformation and fracture mode, and crack–microstructure interactions. Results are analysed in terms of available fracture mechanics models.

2. Experimental procedure

2.1. Materials

The polymer matrices were blends of ABS and styrene–maleic–anhydride (SMA) [22], supplied by Monsanto Chemical Co.. Two levels of butadiene rubber, 9.5 and 2 wt % of the matrix, were studied.

0022–2461 © *1992 Chapman & Hall*

Although a zero rubber-content matrix could have been produced, the addition of 2% rubber made processing easier without significantly affecting the mechanical properties. The rubber particle sizes were also varied. In the 9.5% rubber materials, rubber particles with size about 15 μm (referred to as large particles) together with submicrometre particles were distributed uniformly throughout the samples and will be designated as material A. A different batch containing smaller rubber particles (approximately 4 μm) in combination with submicrometre particles, referred to as material B, was also made. On the other hand, the 2% rubber-containing material contained only the submicrometre particles and will be designated as material C.

Composites were made by dry blending chopped (4.75 mm long) E-glass fibres with matrix materials, and compounding during the injection moulding process. The fibres were 13 μm in diameter and were ~ 300 μm in length after injection moulding. Three levels of glass-fibre content, 5, 10 and 20 wt %, respectively, were achieved. Table I summarizes the material compositions and their designations. Injection moulding of test specimens was carried out at identical conditions for all samples. Samples moulded included ASTM D638 Type I tensile specimens (12.7 mm wide by 3.2 mm thick) and rectangular 12.7 × 6.4 mm thick test bar for the three-point bend test and Izod impact test.

2.2. Characterizations and mechanical tests

Microstructures of specimens were studied using optical microscopy. Specimen surfaces were first polished to a 1-μm surface finish before examination. An optical microscope, Olympus AH2, with differential interference contrast was then used to characterize the microstructural details of the materials. Rubber particle morphology, as well as size distributions, were also characterized by using transmission electron microscopy (TEM).

Tensile tests were carried out according to ASTM D638 on an Instron model 3602 hydraulic testing machine. Displacements were measured using an extensometer attached to the specimen gauge section. A strain rate of 1% min^{-1} was used for all tensile tests. All testing was carried out in room temperature and in ambient air.

2.3. Fracture toughness

Pre-cracked single edge-notched (SEN) specimens were used to determine the J integral fracture toughness at crack initiation, J_{ic}, using the method described by Early and Burns [23]. The controlled pre-cracks with crack length ranging from $a/w = 0.5$ to 0.7 were made by inserting a fresh razor blade into tensile specimens. The specimens were then loaded in tension at a strain rate of 1% min^{-1}. An extensometer was used accurately to record the displacements along the loading line. After crack initiation, which is indicated by a sharp change in the slope of load-displacement curve, the initiation toughness J_{ic} can then be calculated by [23]

$$J_{ic} = \frac{1}{\Delta A}\oint P\mathrm{d}x \quad (1)$$

where ΔA is the difference in crack area of specimens with finite differences in crack length, and $\int P\mathrm{d}x$ is the area enclosed by the load–displacement curve and the line connecting the crack initiation points. Initiation toughness data were also obtained from the R-curve test results (see below).

The crack propagation results, or the material R-curve behaviour, was measured by the ASTM E813 three-point bend test using a pre-cracked 6.4-mm-thick bend bar. The displacement rate used for all three-point bend tests was 1 mm min^{-1}. The specimens were first loaded in bending up to various points of crack advance and unloaded. Specimens were then fast fractured in liquid nitrogen and the crack advance Δa was measured using a stereo microscope. Initiation toughness and the energy spent during the crack propagation, or 'propagation toughness', were then determined by constructing the J–R curve. The specimen thickness of the toughness measurements were also checked by the ASTM recommended values of

$$a, B, (W - a) \geq 25 J_Q/\sigma_y \quad (2)$$

where a is the pre-crack length, B is the thickness, W is

TABLE I Materials' composition and designation

Material designation	Rubber (wt %)	Glass Fibre (wt %)	Particle size
Matrix A	9.5	—	15 μm and submicrometre
Composite A5	9.5	5	" "
A10	9.5	10	" "
A20	9.5	20	" "
Matrix B	9.5	—	4–5 μm and submicrometre
Composite B5	9.5	5	" "
B10	9.5	10	" "
B20	9.5	20	" "
Matrix C	2	—	submicrometre
Composite C5	2	5	" "
C10	2	10	" "
C20	2	20	" "

the width of the specimen and J_Q and σ_y are the initiation toughness and the materials's yield stress, respectively. It was found that the thickness requirement was satisfied for all specimens except in the two cases of 9.5 wt % rubber-toughened materials A and B with no glass. Unfortunately, attempts in injection moulding thicker samples failed due to non-uniform shrinkage in the specimen width. In these two cases, only the toughness data from the three-point bend test with 6.4-mm-thick samples are obtained.

Notched Izod impact testing was carried out according to ASTM D256 procedure with 3.2-mm-thick specimens. A Zwick Izod impact tester was used with a 2.7 J striker. The pendulum velocity in this test at the point of impact is 3.5 m s^{-1}, and results are reported as the total energy absorbed during impact.

2.4 Fracture observations

In situ fracture observations were carried out by using a buckled-plate fixture [24] placed under an optical microscope, as shown in Fig. 1. The advantage of using the buckled-plate fixture is that the crack driving force is independent of crack size [24]. Thus by observing the crack propagation under an optical microscope, the fracture micromechanisms under a constant stress intensity factor can be recorded.

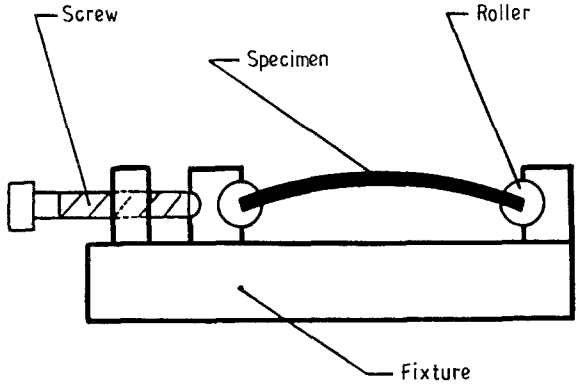

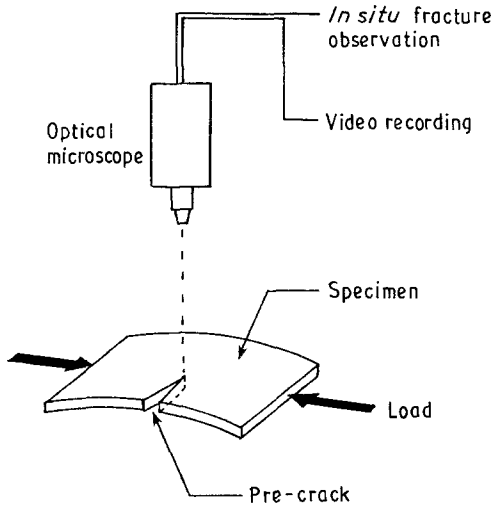

Figure 1 Schematic diagrams of the buckled-plate fixture [24] and the experimental setup for *in situ* fracture observations.

Pre-cracked specimens with polished surfaces were loaded in the buckled-plate fixture up to the point of crack initiation. The fracture processes were then observed by using differential interference contrast microscopy, and were also video recorded for further analysis.

The fracture surfaces were examined by SEM in a Jeol JSM-5200 electron microscope after fracture of the specimens.

3. Results and discussion

3.1. Microstructures

The optical and TEM micrographs of material A, which contains 9.5 wt % rubber particles (see Table I), are shown in Fig. 2a and b, respectively. The particle morphology and internal sub-inclusion structures [25] in the rubber particles are clearly identified. Similar observations for materials B and C are also shown in Figs 3 and 4, respectively. Note that in materials A and B two major particle distributions, the submicrometre and the supermicrometre particles, are presented whereas in material C only the submicrometre particles are found. Exact determination of rubber particle volume fractions was not made, due to difficulties raised by the complex internal occlusion structures of the particles [26]. However, estimation of the rubber particle volume fraction for material A including occluded particles, and measured by a point counting technique, is approximately 18%.

Typical microstructures of the composites A, B and C are seen in Fig. 5a–c, respectively. Note that the morphology of rubber particles and their size distributions are not changed as the glass fibres are added, and no agglomeration of rubber particles onto the fibre/matrix interface can be identified. Similar fibre distributions and fibre aspect ratios are also observed in all three composite systems. As the fibre content increases it is found that the glass fibres tend to form bundle-like clusters during injection moulding, which produces higher degrees of non-uniformity within the composites. The tendency for fibre break-down by injection moulding is also increased as the fibre content increases.

3.2. Tensile mechanical properties

The mechanical properties of the materials studied are summarized in Table II. The stress–strain curves of the matrix materials A, B and C are shown in Fig. 6. Note that in the rubber-toughened materials A and B, the increase in ductility is dramatic and is accompanied by stress whitening throughout the specimens in the plastic portion of the stress–strain curve. A close examination of the polished tensile surface of material A specimens, as shown in Fig. 7, clearly reveals that the crazes induced by rubber particles are the main source for the stress whitening and the observed ductility increase. Also in Fig. 7 it can be seen that larger rubber particles and the particles with elongated morphology are able to induce more crazing, possibly due to their high misfit strains [16]. Similar observations of crazing associated with rubber particles on the tensile surface of material B were also

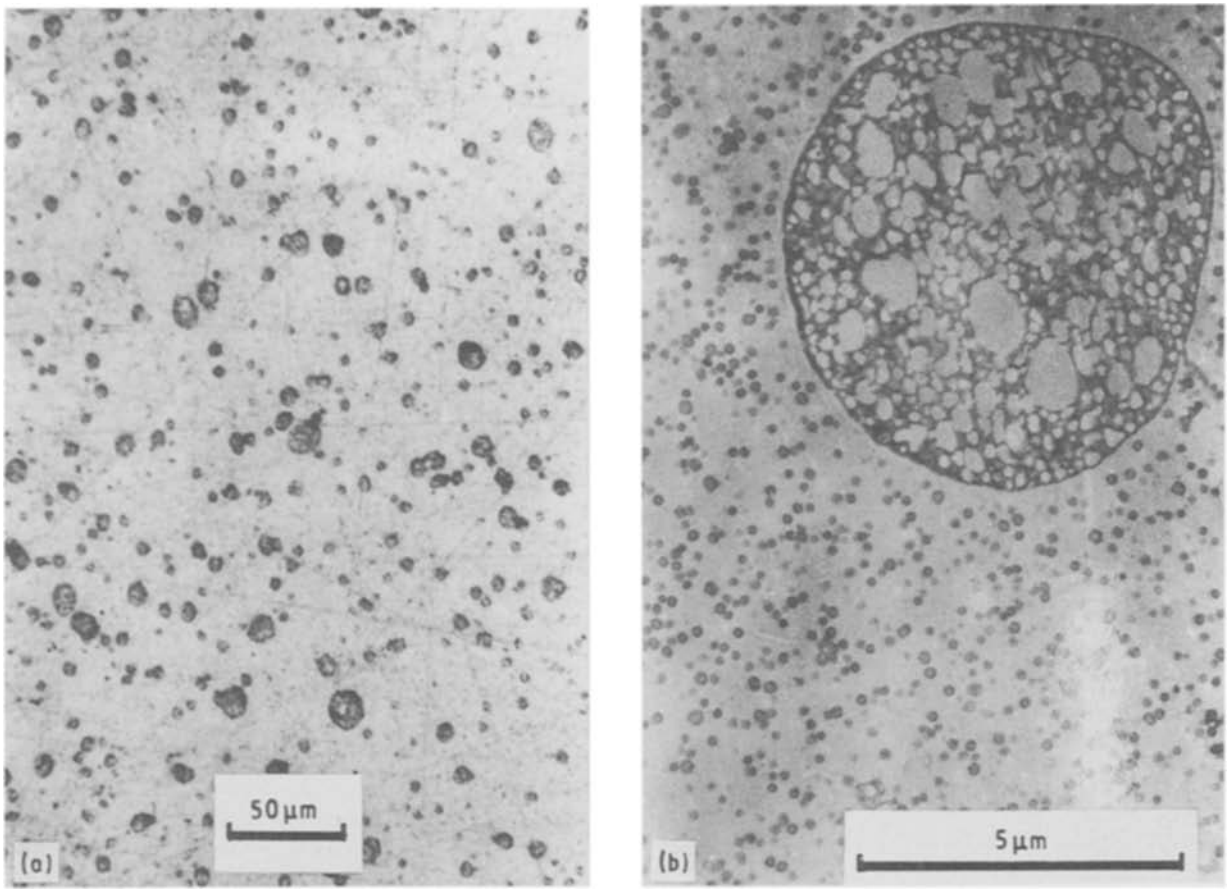

Figure 2 Microstructures of the 9.5 wt % rubber-toughened material A (large rubber particles). (a) Optical micrograph; (b) TEM micrograph.

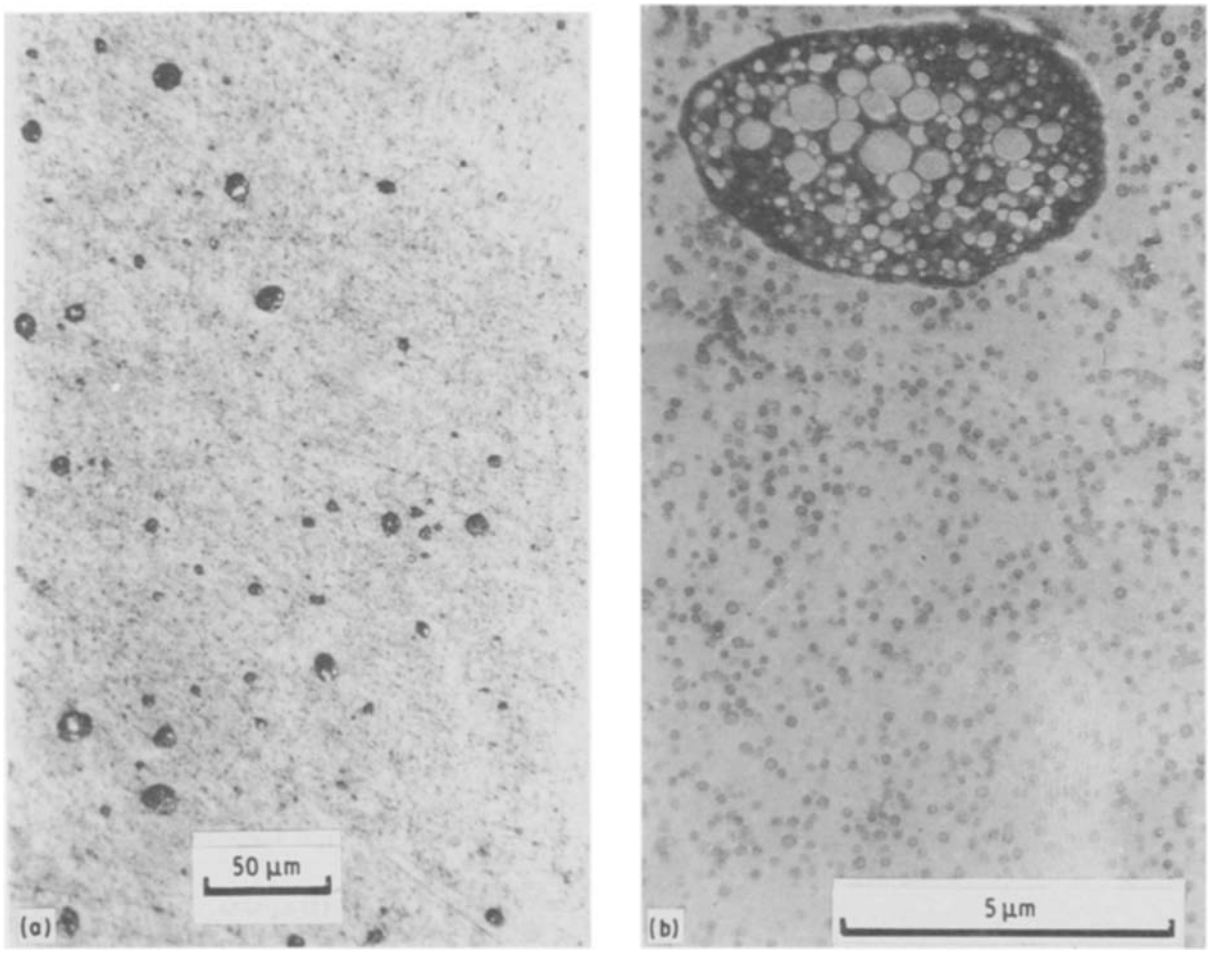

Figure 3 Microstructures of the 9.5 wt % rubber-toughened material B (small rubber particles). (a) Optical micrograph; (b) TEM micrograph.

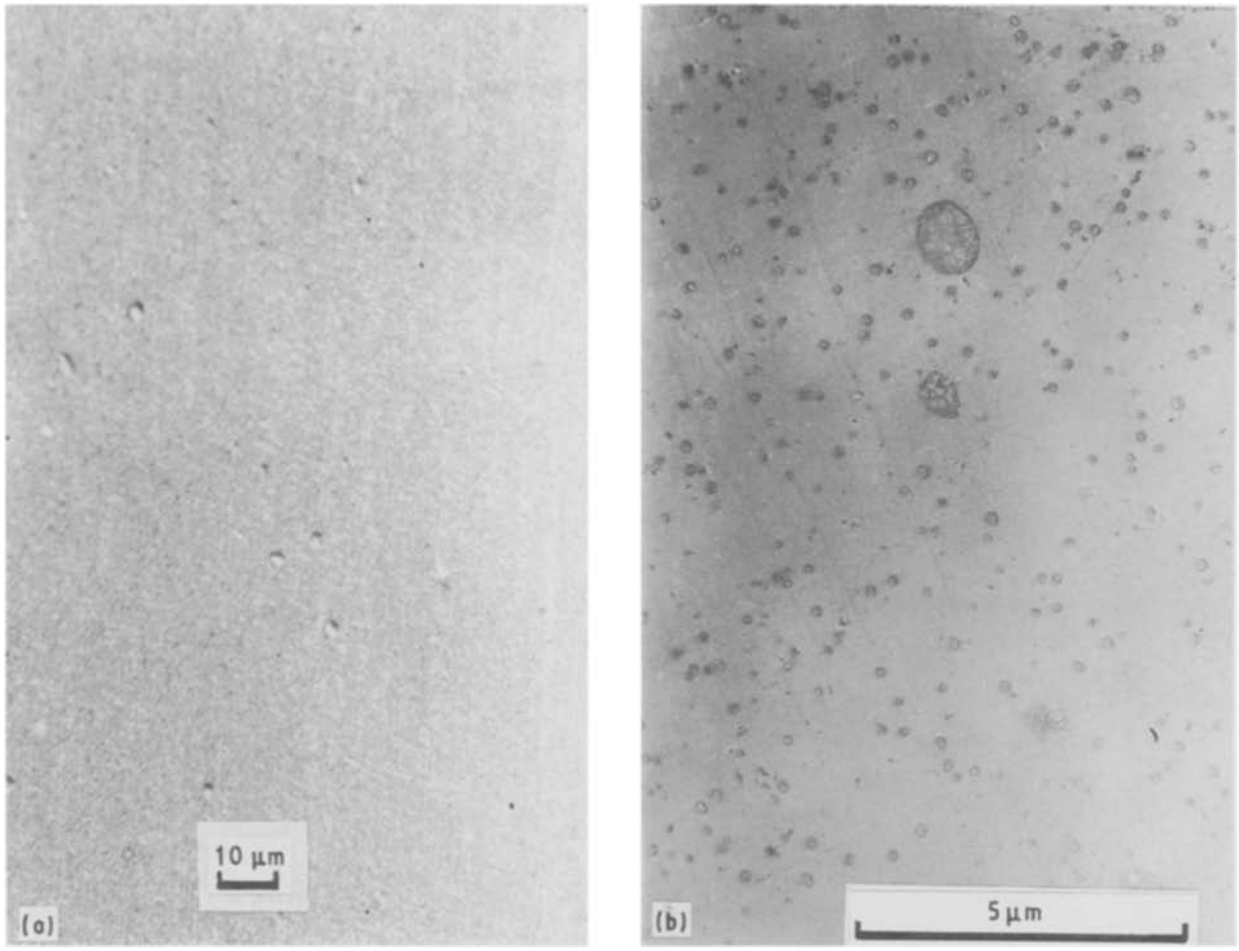

Figure 4 Microstructures of the untoughened material C. (a) Optical micrograph; (b) TEM micrograph. In (a) the surface of the samples has been etched by chromic acid for 10 h at room temperature to reveal the submicrometre particles.

found. However, additional studies of volume change during tensile deformation (Fig. 8) suggest that material B may exhibit a slight decrease in the amount of crazing. Nevertheless, the slight reduction in the crazing amount alone cannot fully explain the observed significant difference in the ductility between material A and B.

In the composite systems it is found that the increase in ductility with rubber particle additions is much less than for the case of the unreinforced matrix materials. The results are shown in Fig. 9, where the stress–strain curves of composites with 10 wt % fibres are depicted. Similar results were also obtained in other levels of fibre-containing composites. The change in ductility, or the strain at break, is best demonstrated in Fig. 10, where the strain at break is plotted as a function of glass-fibre content. As can be seen, the ductility is decreased by a factor of 10 in composite A and by about a factor of 5 in composite B, with only 5 wt % glass addition. However, further increases in fibre content do not produce any significant decrease in ductility. In the untoughened composites, on the other hand, the ductility shows a weak dependence on the glass-fibre content. An optical examination of the tensile surface of the toughened composite A10 (10 wt % glass fibres) shows that crazing at rubber particles is inhibited. Also, no significant stress whitening on the tensile surface could be identified. These results indicate that the presence of only small amounts of fibre reinforcement can severely decrease the bulk ductility of a rubber-toughened thermoplastic, through its corresponding influence on limiting crazing or shear yielding around the rubber particles.

TABLE II Mechanical properties

Material	Yield stress (MPa)	Young's modulus (MPa)	Strain at break (%)
A	34.34	1417.6	24.75
A5	45.85	1880.2	3.288
A10	55.49	2327.2	2.937
A20	76.57	2596.4	2.425
B	36.37	1557.3	13.769
B5	45.29	1775.2	3.23
B10	59.24	2295.0	2.81
B20	72.39	2769.5	2.3
C	44.61	1734.6	2.12
C5	54.04	2069.2	1.63
C10	63.92	2462.9	1.575
C20	72.17	2740.4	1.41

3.3. *In situ* observations of deformation and fracture ahead of crack tips

The fracture behaviour of the untoughened and toughened matrices both with and without glass fibres

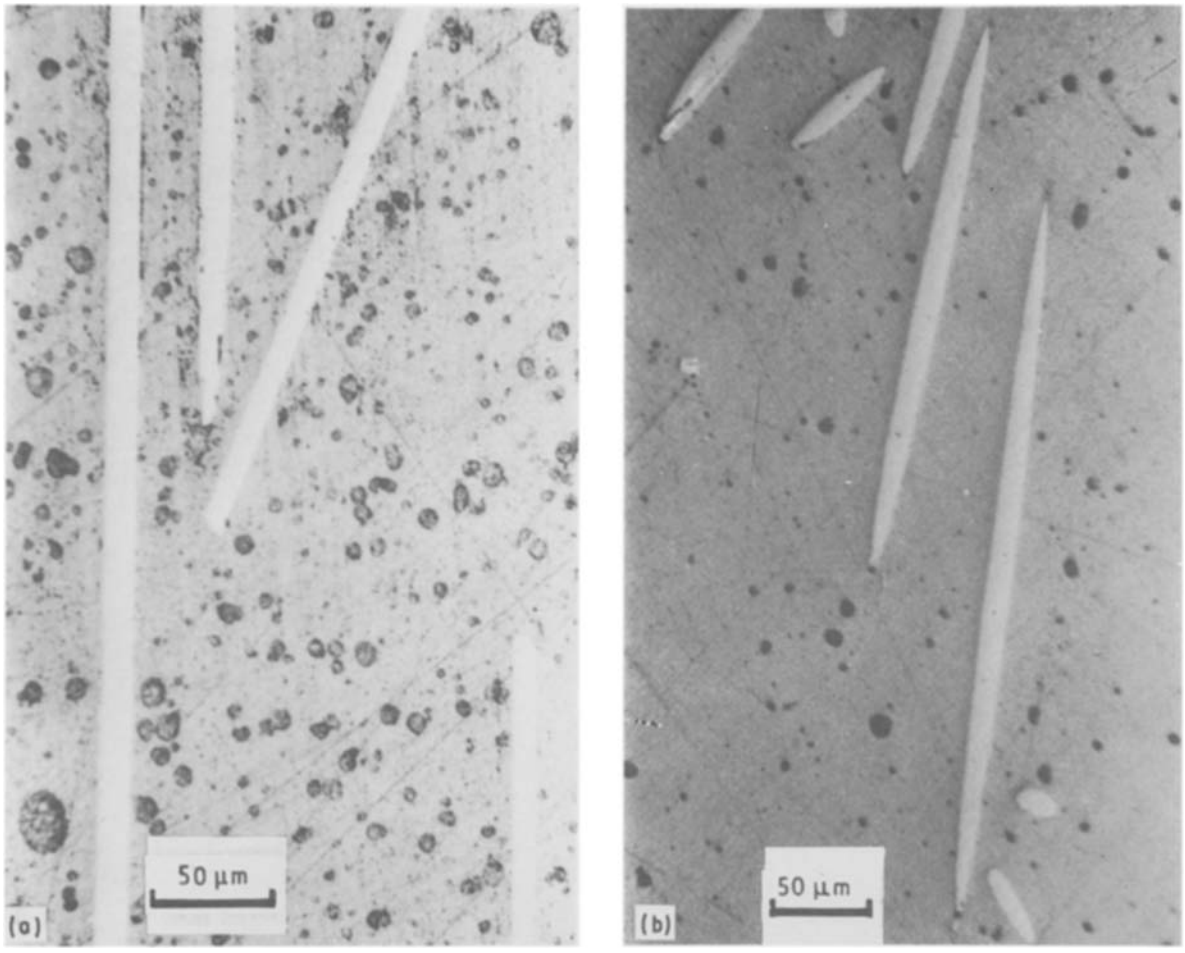

Figure 5 Optical micrographs for the microstructures of the composites with 10 wt % glass-fibre addition. (a) Composite A10; (b) composite B10; (c) composite C10.

was observed *in situ* by loading pre-cracked samples to failure as described (see Section 2.4). It was found that in the untoughened material C the crack tip is blunted by the noticeable formation of shear bands initiated from the crack tip at an angle of about 55°, as shown in Fig. 11. This figure also shows limited crazes in front of the crack tip at the direction perpendicular to the loading direction. Further *in situ* examinations on the untoughened material C suggest that failure is dominated by a shear type of fracture, indicated by breakdown of shear bands [27] and diamond cavitation at limited crazes in front of the crack tip [28, 29].

In the toughened matrices a significant difference in fracture modes is observed. It is found that in the case of matrix material A, a large volume of crazes initiated from rubber particles can be identified in the crack tip plastic zone before crack propagation, as shown by the whitening zone in Fig. 12. In the small rubber-containing material B, in addition, shear bands associated with small rubber particles were observed, as

clearly shown by the criss-cross pattern in Fig. 13. The crack tip then advances with a constant crack flank angle by linking up along the path of crazes associated with those largest particles within the crack plane. Crack impingement at rubber particles and consequent tearing of the particles were also observed. Fig. 14 shows the SEM evidence of rubber particle tearing on the fracture surface of material A. The net result is one whereby crack advance in the rubber toughened matrices occurs by the breakdown of crazes at large particles followed by subsequent tearing of these rubber particles.

In the composites, localized craze deformation initiated more readily in the crack tip plastic zone than in the bulk tensile samples (see Fig. 15). This is consistent with the presence of sharp stress gradients in

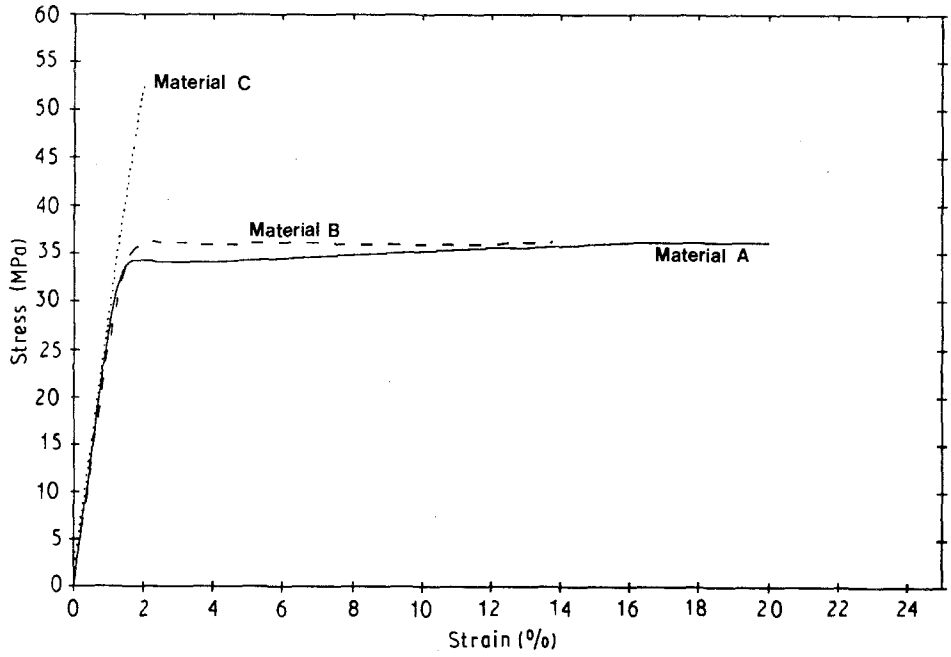

Figure 6 Stress–strain curves for the matrix materials A, B and C.

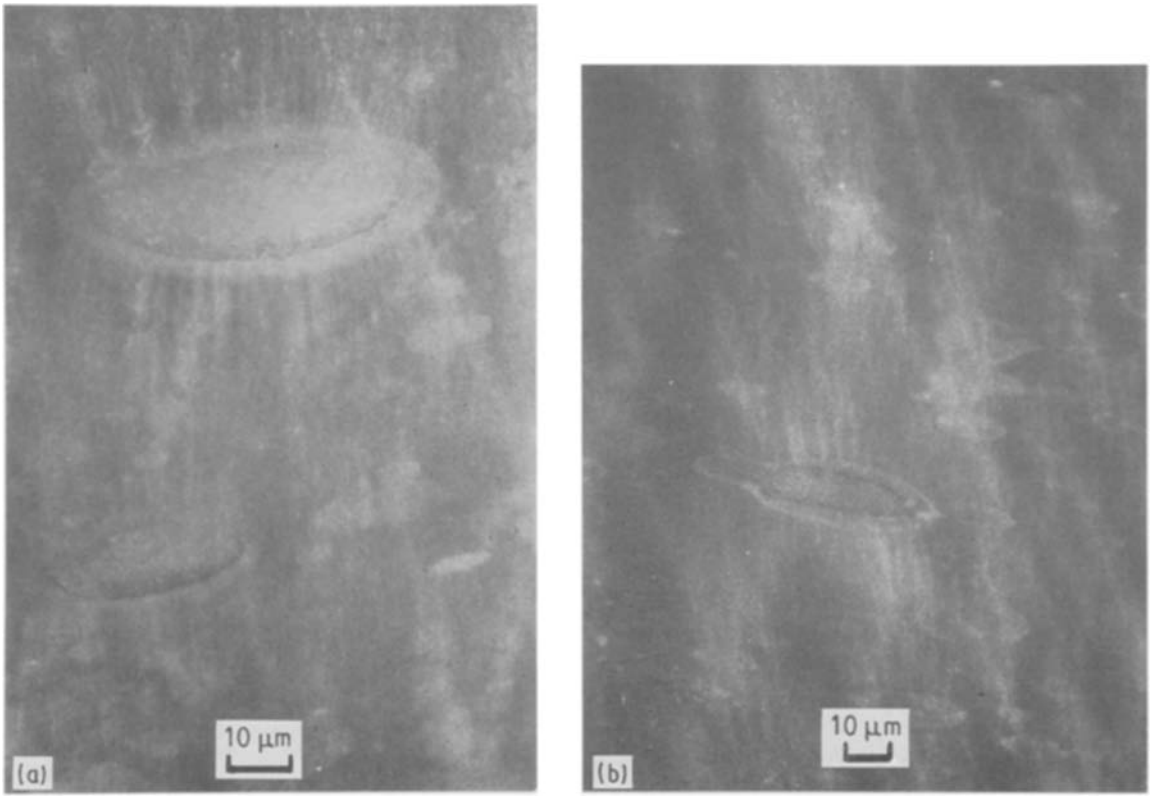

Figure 7 Optical micrographs of the deformed tensile specimens toughened by large rubber particles (material A). The crazes initiated at rubber particles were revealed by differential interference contrast in (a) and shown in enlarged magnification in (b).

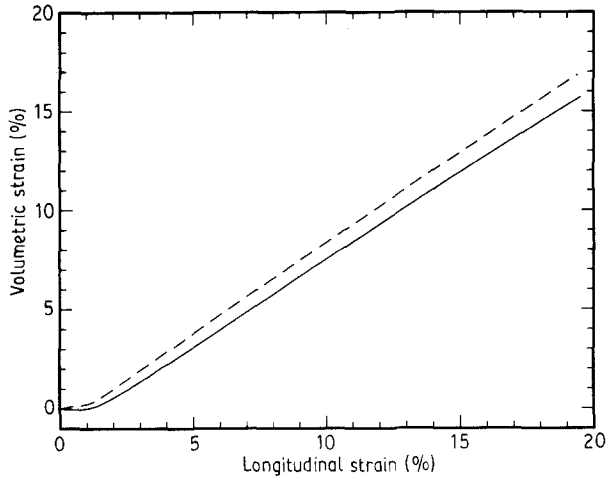

Figure 8 Volumetric change during tensile deformation for materials (---) A and (—) B. The amount of crazing is estimated from the slope of the curve [36] and is 91.7 ± 1.5% for material A; 88.2 ± 1.7% for material B.

the crack-tip zone which would prevent stress shielding of the matrix by the glass fibres observed in the bulk tensile samples in the presence of uniform tension. Further, rubber particles are subjected to the triaxial stresses of the crack tip zone, thereby enhancing craze growth which is a dilatational process [15, 16].

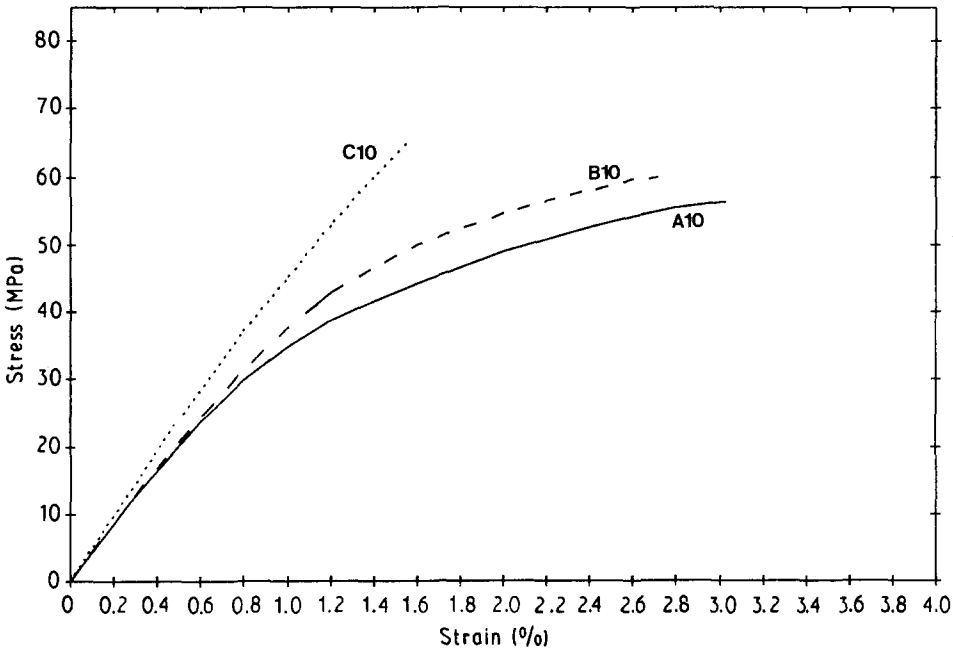

Figure 9 Typical stress–strain curves for the composite materials A10, B10 and C10.

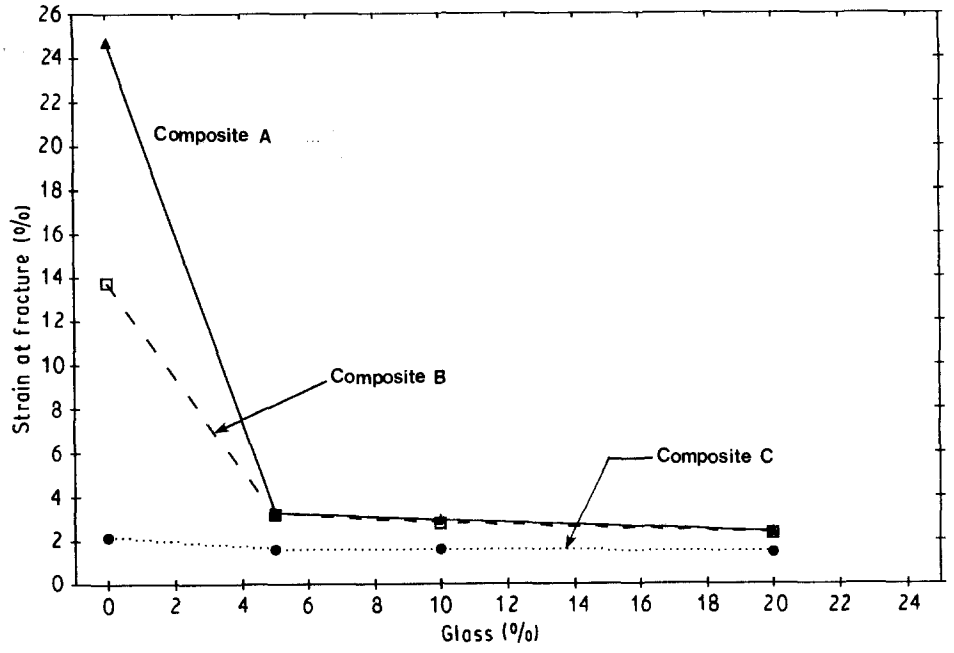

Figure 10 Ductility or the strain at break against glass-fibre content for the composite systems A, B and C.

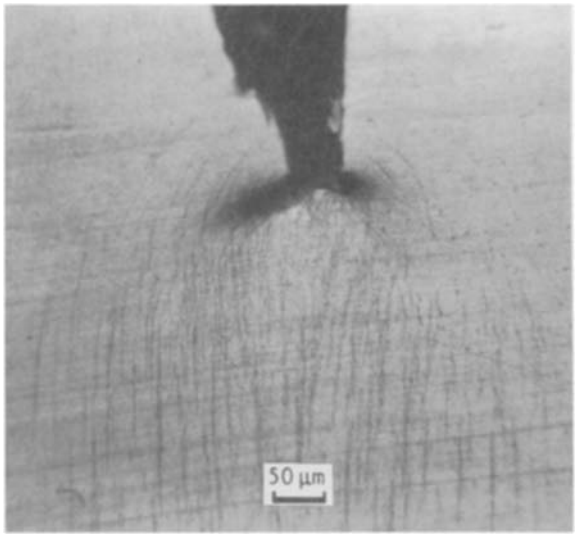

Figure 11 Shear-band formation at the crack-tip region of the untoughened material C. Further crack-tip advance is followed by thickening and breakdown of the shear bands.

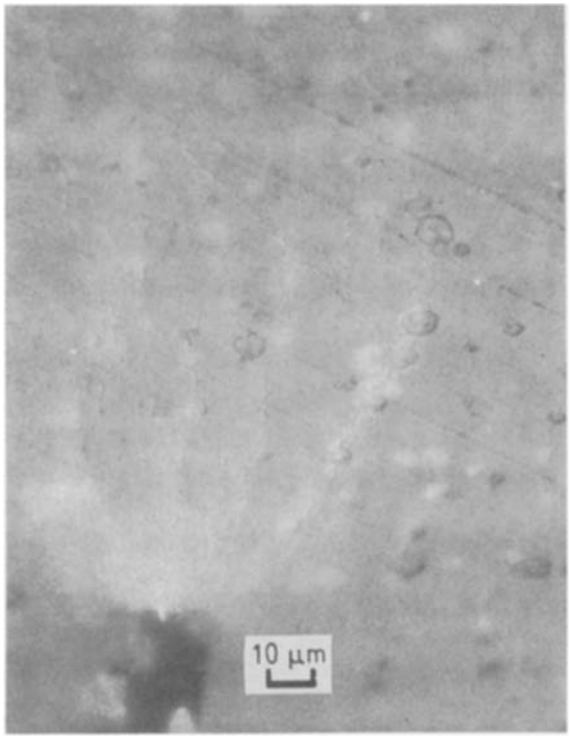

Figure 12 Craze formation at large rubber particles in the crack-tip plastic zone of rubber-toughened material A.

In the presence of the glass fibres, crazing is initiated not only at the rubber particles, but extensive crazing is also initiated at the glass fibre/matrix interfaces. In Fig. 16 the crazes appear to initiate and progress along the slip line or shear field around the glass fibres. Although crazing is a dilatational process, craze initiation is governed by deviant stresses [16], and consequently shear loading of the glass fibres would promote craze formation at glass fibre/matrix interfaces. However, high shear stresses at fibre/matrix interfaces is not alone sufficient for interface crazing, because such crazing is not observed in the untoughened composites. The untoughnened composites have

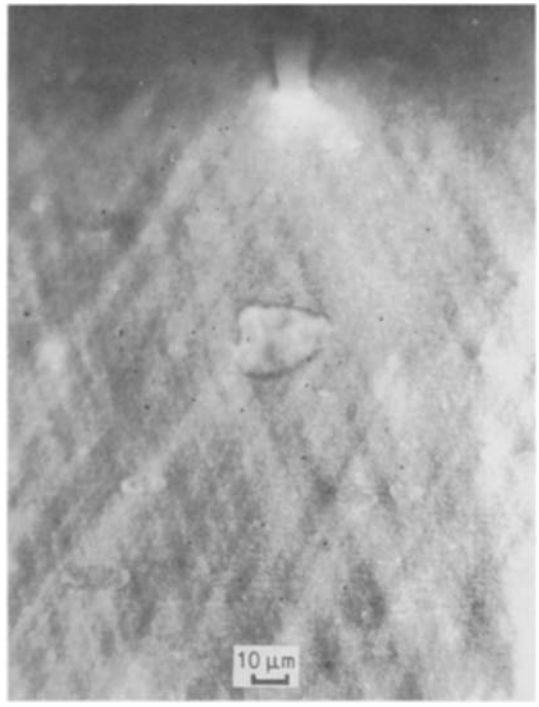

Figure 13 Shear band initiated at small particles in the crack-tip region of material B.

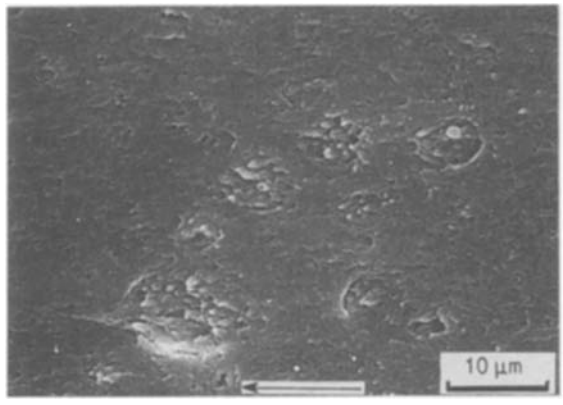

Figure 14 SEM fractography of the rubber-toughened material A indicating the evidence of rubber particle tearing. Arrow shows direction of crack propagation.

Figure 15. Micrograph of *in situ* fracture observation in composite A10 showing limited crazes formed at rubber particles before crack initiation.

higher yield stresses and hence are expected to have higher shear stresses at the fibre/matrix interfaces. Interface crazing requires a combination of rubber particles of sufficient size and volume fraction in

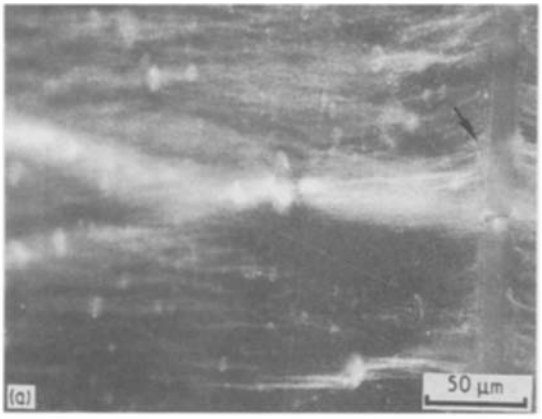

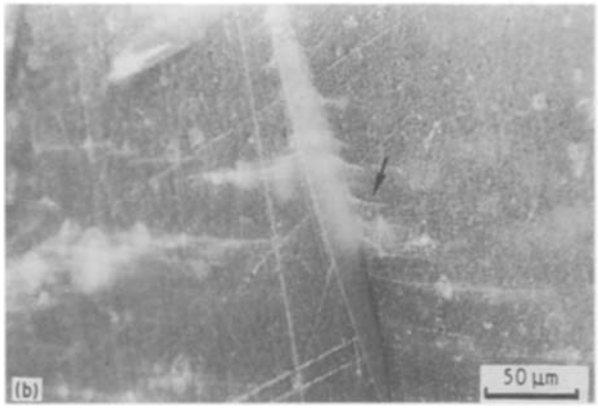

Figure 16 Micrograph of *in situ* fracture observation in composite A10 showing crazes formed at fibre–matrix interfaces, indicated by arrows in (a) and (b).

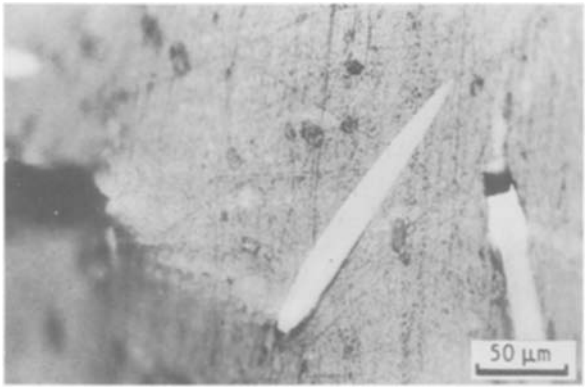

Figure 17 Micrograph of *in situ* fracture observation in composite A10 showing debonding and void formation at fibre ends.

addition to high interface shear stresses generated by shear loading.

Failure in the crack tip region of the rubber-toughened composites is associated first with void formation at glass-fibre ends, (see Fig. 17), followed by fibre-matrix debonding and diamond cavitation in the matrix associated with matrix crazes, (see Fig. 18). Further crack extension leads to fibre pull-out and fibre bridging in the crack wake, (Fig. 19). The crack path is also deflected in a zig-zag fashion by the presence of the fibres. SEM observations on the fracture surface of toughened composites (Fig. 20) show fibre debonding and pull-out, but also show clear evidence of rubber particle tearing within the matrix.

Figure 18 Micrograph of *in situ* observation in composite A10 showing that crack advances by linkage of voids at fibre ends.

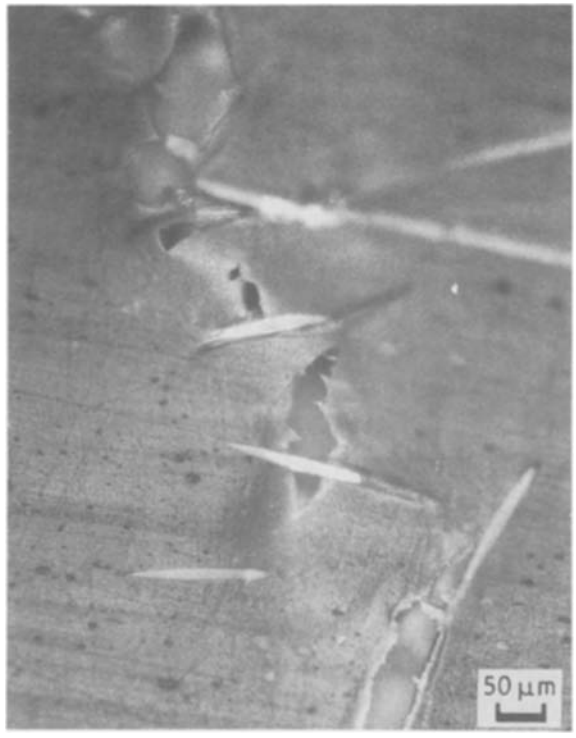

Figure 19 Micrograph of *in situ* observation of crack propagation in composite A10 showing the crack surface is bridged by unbroken fibres.

In the non-rubber-toughened composite C, failure is brittle in nature with little deformation observed in the crack-tip region prior to crack extension associated with stress-concentrating fibre ends (Fig. 21). Further crack growth occurs by linkage of voids formed in advance of the crack tip (Fig. 22).

A feature of the *in situ* observations is the presence of a strong time dependence on the fracture process in

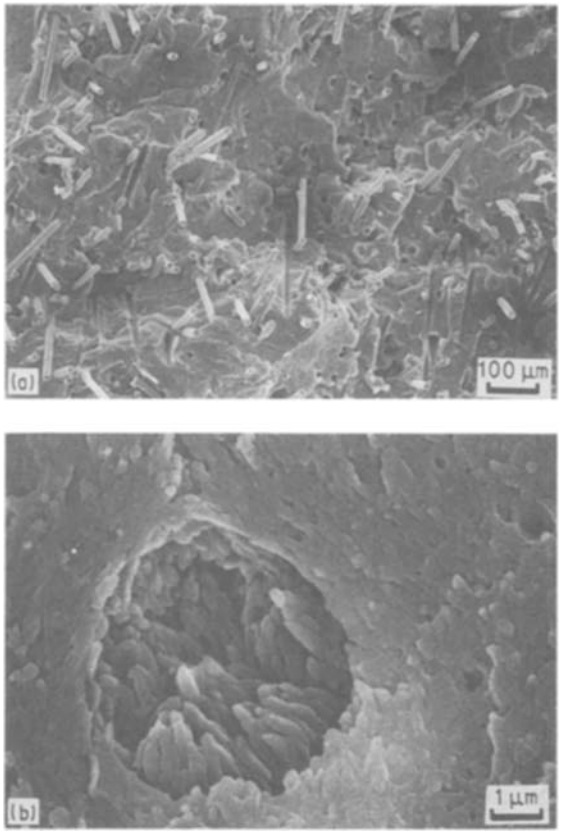

Figure 20 SEM fractography of the composite A10 showing (a) fibre pull-out and (b) rubber particle tearing in the matrix.

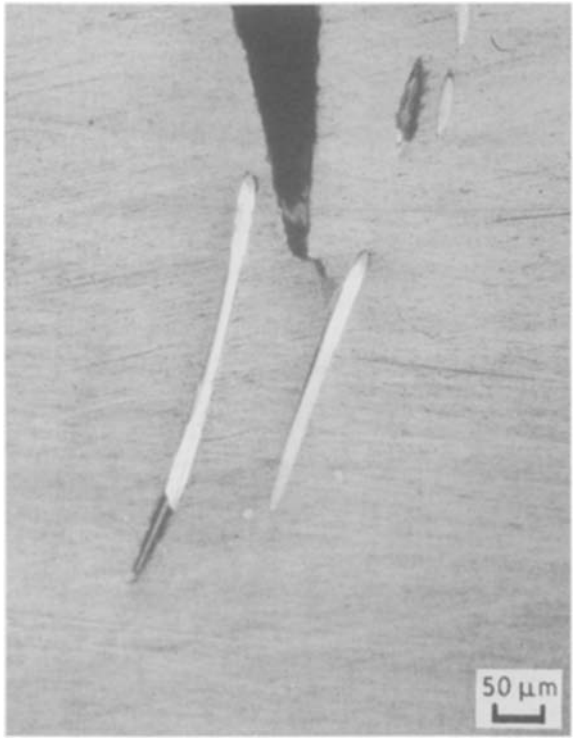

Figure 21 Micrograph of *in situ* fracture observation in the untoughened composite C10 showing crack-tip advance with little plastic deformation.

all materials. In other words, at a constantly applied stress intensity to the buckled-plate loaded materials, time-dependent crack advance and void formation were observed. Voids which formed at craze sites or

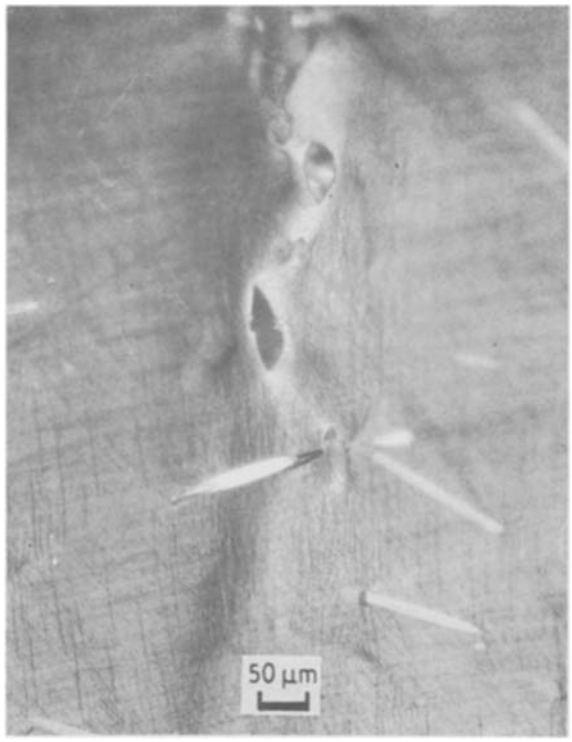

Figure 22 Micrograph of *in situ* observation of crack propagation in composite C10 indicates void formation at fibre ends and diamond cavitation in the matrix.

fibre ends grew in size with time before linkage and crack extension. This time-dependent crack growth associated with the viscoplastic matrix deformations is not accounted for in the toughness measurements (see below) since the loading rates used for these measurements were sufficiently rapid.

3.4. Fracture toughness

3.4.1. Initiation toughness

In Fig. 23, the initiation toughness J_{ic} of the materials studied is plotted as a function of glass-fibre content. It is found that in the composites with rubber modifications, the initiation toughness is significantly higher than that of the composites without rubber modification. Although the magnitude of the toughness increase due to rubber addition is decreased at higher glass-fibre volume fractions, the increase is still substantial. Furthermore, the composites with larger rubber particles result in larger toughness increases. Note also that glass-fibre additions increase the initiation toughness of untoughened composite C but initially decreases the toughness of the rubber-toughened composites A and B. Beyond about 10 wt % fibres, however, the initiation toughness of all composites are increased.

The initiation toughness can be related to the tensile yield strength, σ_y, and ductility, ε_f, provided failure in a hypothetical microtensile specimen at the crack tip occurs in the same manner as for macroscopic tensile specimens. Then

$$\varepsilon_f \approx \frac{COD}{2\rho_0} = \frac{J_{ic}}{2\alpha\sigma_y\rho_0} \quad (3)$$

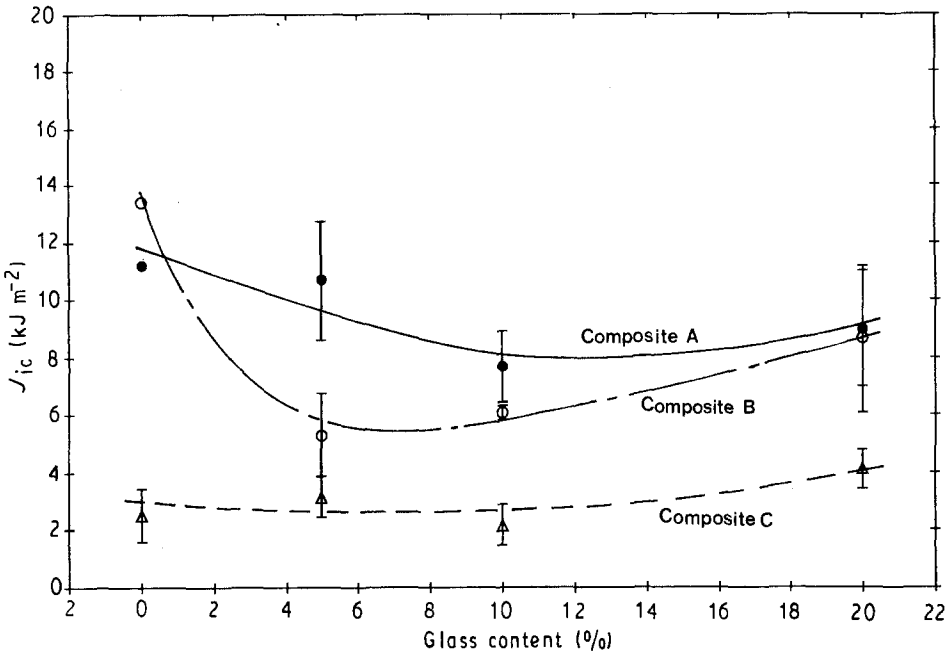

Figure 23 The initiation toughness against glass-fibre content for the composite systems A, B and C.

So that

$$J_{ic} \approx 2\alpha\varepsilon_f\sigma_y\rho_0 \quad (4)$$

where *COD* is the crack opening displacement at crack initiation; $J_{ic} = J$ is integral toughness at crack initiation; ρ_0 is the crack-tip radius at crack initiation; and α is a constant, which is close to a unity [30]. Thus, according to this simple model, initiation toughness is proportional to the product of the strength and ductility of the material. Fig. 24 shows predicted curves using Equation 4 for the initiation toughness as a function of glass-fibre content superimposed on the measured data. For the untoughened matrix, the predicted curve compares well with the measured values. The measured increase in initiation toughness as a function of fibre additions to the untoughened matrix is therefore related to the strengthening effect of the glass fibres.

For the toughened matrices, particularly the large rubber particle case (Fig. 24b), the predicted curves underestimate the composite initiation toughness when glass fibres are added to the matrix. This is consistent with the *in situ* observations discussed above. In the crack tip, due to the presence of stress gradients, the localized craze deformations at rubber particles are not as inhibited by glass as in the tensile tests. Furthermore, additional craze energy is dissipated at the fibre/matrix interfaces.

Note that the decrease in measured toughness with glass fibre additions is more substantial for the small rubber particle case. This is also consistent with the *in situ* observations of greater levels of shear rather than craze deformations due to the presence of the smaller rubber particles. Impingement of the shear bands at glass fibres can promote void formation at fibre ends and decrease initiation toughness. Finally, the increase in the initiation toughness of both toughened matrices as the glass-fibre content is increased further is due to the strengthening influence of glass fibres. As observed earlier (Equation 4) J_{ic} is proportional to the composite yield strength.

3.4.2. Propagation toughness

The J_R–Δa curves for the rubber-toughened materials A and B are shown in Fig. 25. For the large rubber particle material A, the crack-growth resistance starting from initiation toughness (0.2 mm blunting line) is seen to increase by more than a factor of 2, whereas for the small rubber particle material B, this increase is somewhat less. In both cases, however, the propagation component of toughness is of the order of the initiation toughness component.

The J_R–Δa curves for the 5, 10 and 20% glass-fibre contents were only obtained for the large rubber particles and are shown in Fig. 26. The propagation component of toughness is approximately the same for all three fibre contents and, in all cases, its magnitude is of the order of the initiation toughness component. Note also that the magnitude of the crack-growth resistance increase is the same as that for the rubber-toughened matrix without the glass fibres.

The increase in the crack-growth resistance with Δa for the rubber-toughened material A without the glass fibres clearly indicates that substantial additional toughening can be obtained from crack-wake effects in the presence of rubber particles. This study provided evidence for two observed crack-wake effects. The first is the rubber particle bridging of cracks, discussed above that was supported by the SEM and *in situ* observations. The second is the presence of a stress-whitened craze deformation zone in the crack wake (Fig. 27). As discussed by Evans *et al.* [31], the wake zone exerts a closure pressure on the crack faces because unloading of crazes in the crack wake results in a zone of residual deformation.

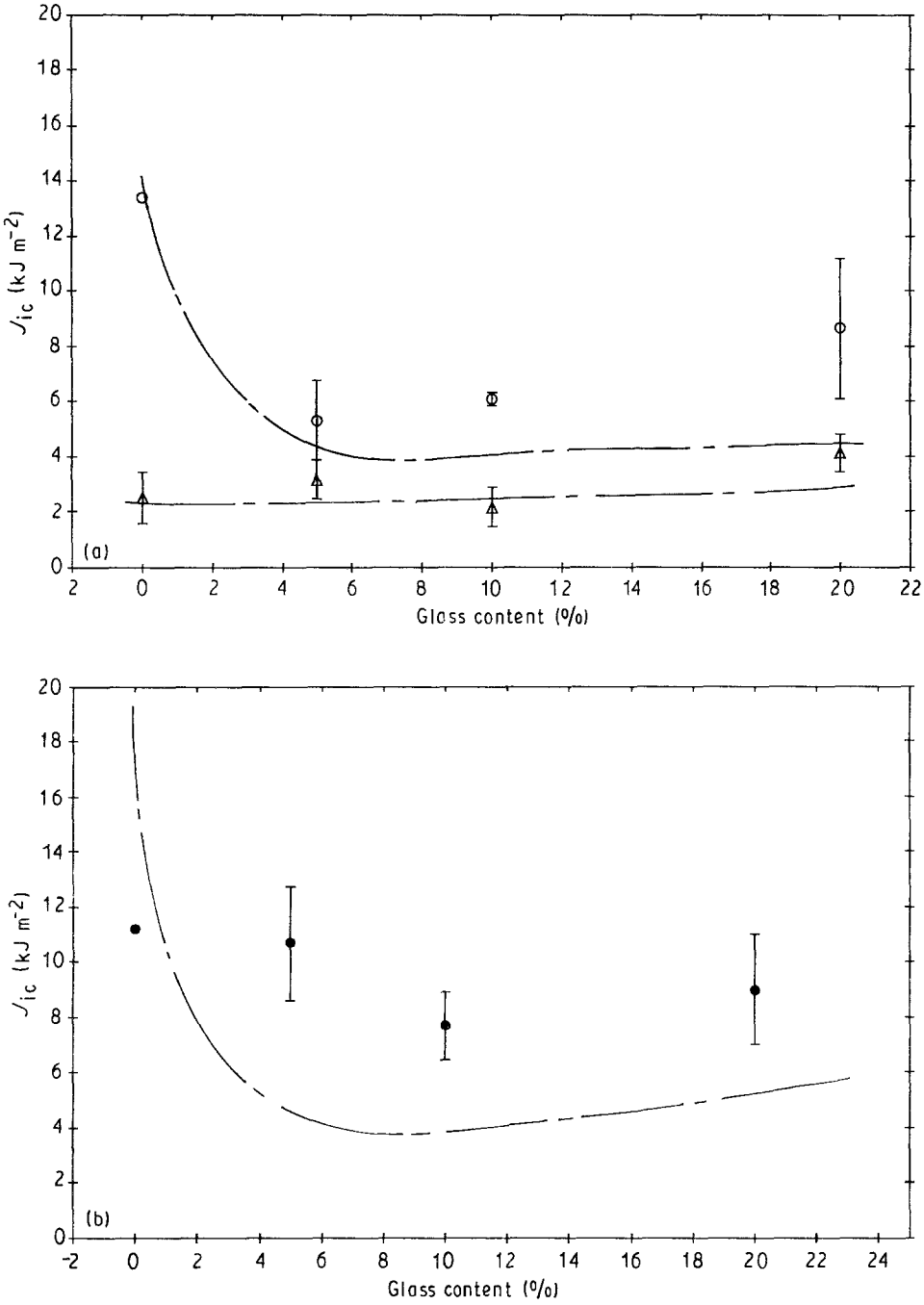

Figure 24 Comparison of the theoretical predictions (— · —, Equation 4) with the experimental values from this study. (a) Composites ○, B and △, C; (b) ●, composite A.

The steady-state toughness increase, J_s/J_i, where J_i is the initiation toughness, can be given by [32]

$$\frac{J_s}{J_i} = \frac{\mu f \langle R \rangle}{J_i}\left(\lambda_f^2 + \frac{2}{\lambda_f} - 3\right) \quad (5)$$

where μ is the shear modulus of rubber. Using $\mu \simeq 1$ MPa, $f \simeq 0.2$, $\langle R \rangle = 10$ μm and a large value of λ_f of 10

$$\frac{J_s}{J_i} = 7.78\% \quad (6)$$

Thus only relatively small increases in toughness appear to be predicted by rubber particle bridging alone. We therefore conclude that dilatational crack-wake effects may play an important role in the observed propagation toughness. Unfortunately, at the present time no model for craze dilatational toughening in the crack wake is available. Work on such a model is in progress [33] based on the original analysis of Evans *et al.* [31].

With regard to propagation toughness in the presence of glass fibres, because of the significantly reduced craze deformations in the crack tip plastic zone, the dilatational toughness component is expected to be small. In fact, the craze-zone height on either side of the crack plane is much smaller than in the absence of glass fibres which would predict that dilatational wake toughening would indeed be significantly reduced [31]. Accordingly we attribute the observed large increase in J_R with crack extension predominantly in terms of the bridging of matrix cracks by fibres, fibre pull-out and crack defection effects.

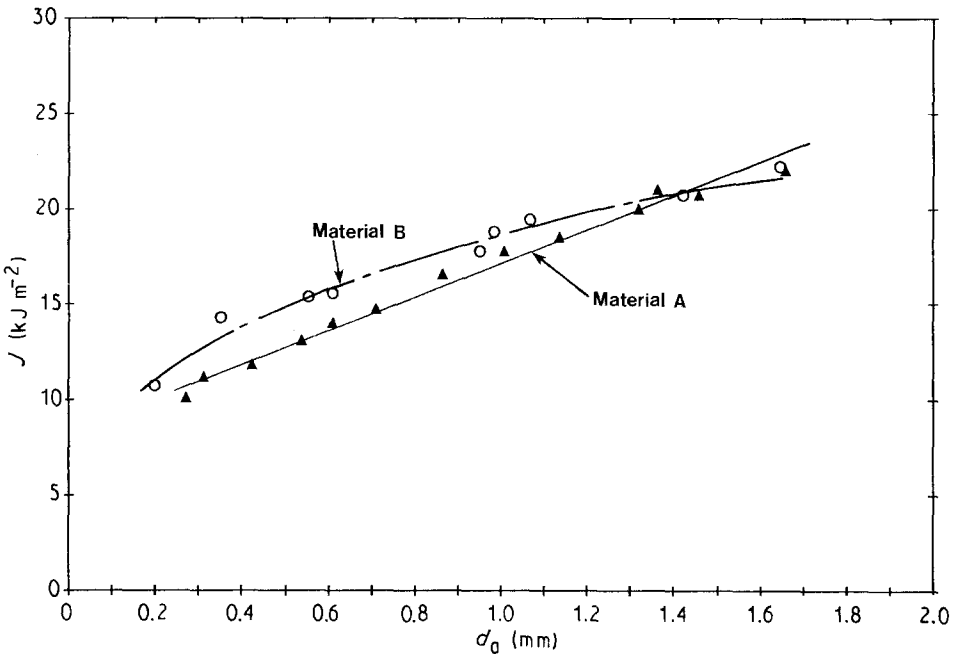

Figure 25 J–R curves for the rubber-toughened materials A (▲) and B (○).

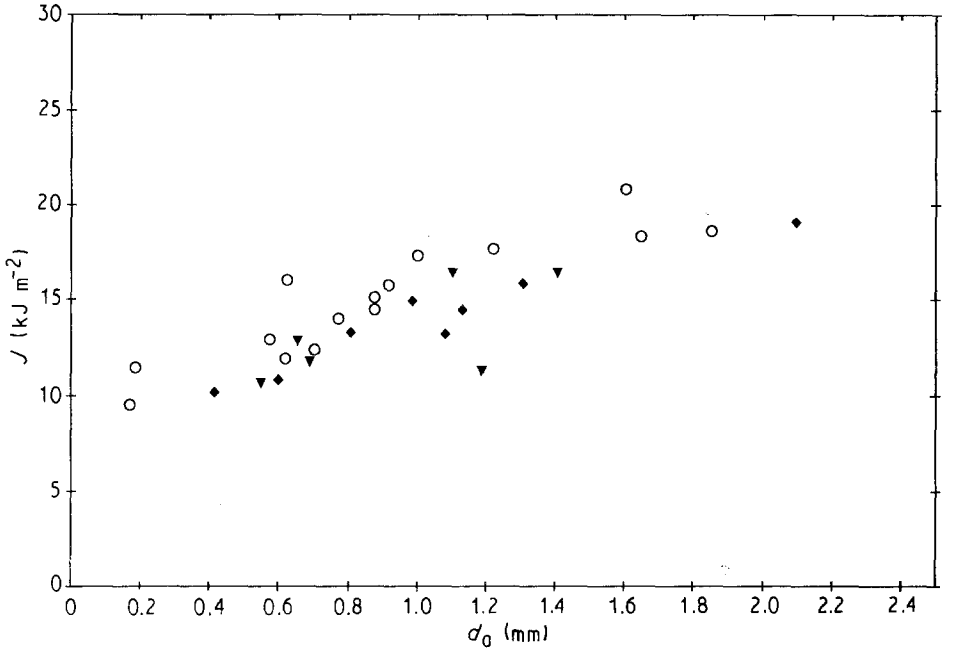

Figure 26 J–R curves for the rubber-toughened composites ○, A5; ◆, A10; and ▼, A20.

3.5. Impact toughness

The results of Izod impact testing on the composite A, B and C are shown in Fig. 28 as a function of glass-fibre content. As in the case of initiation toughness, it is found that the rubber-toughened composites show a significant increase in impact toughness as compared to the untoughened composite C. Note that in composites B and C the Izod toughness shows a monotonic increase with fibre content, whereas in composite A the Izod toughness shows a weaker dependence on fibre content, with a slight drop in toughness in the low glass fibre range. Also note that in cases of rubber-toughened materials A and B (0% glass fibre), a large difference in the Izod toughness is observed, with the smaller rubber particles being much less efficient in toughening the material under high strain-rate loading. Another difference in the Izod results is the much larger increase in toughness of the untoughened composite C with fibre additions when compared with the slow strain rate toughness results.

The Izod test results are representative of a combination of initiation and propagation toughness under high strain-rate-loading conditions. Under these conditions, void formation at fibre ends which, as discussed, was a time-dependent process, can be suppressed. This can explain the smaller decrease in toughness with fibre additions to the toughened material A. The large increase in toughness of the untoughened material C may be explained in terms of the much larger increase in composite strength at high

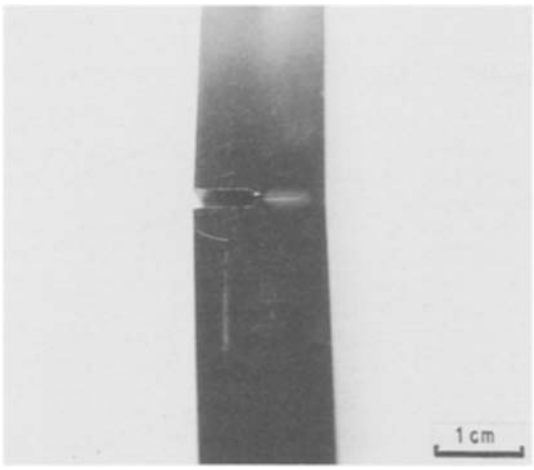

Figure 27 Stress-whitening zone in the crack wake of rubber toughened material A.

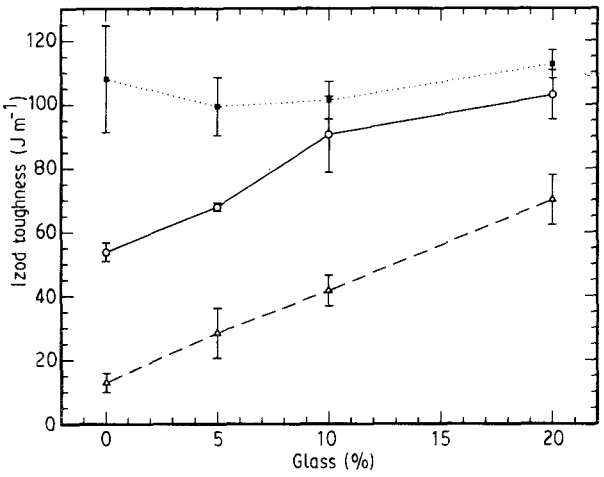

Figure 28 The Izod impact toughness against glass-fibre content for the composite systems ■, A, ○, B and △, C.

loading rates. In the absence of a more detailed study on the influence of strain rate on toughening mechanisms these are only tentative but plausible interpretations.

3.6. Implications for fibre/matrix interface requirements

The results of this study leave open the question of whether a strong or a weak fibre/matrix interface is necessary for toughening of the rubber particle-containing matrices. In fibre-reinforced thermoset composites, a high-strength interface is usually detrimental to toughness as it allows cracks to propagate through the reinforcing fibres [34, 35]. A weak interface is more desirable in order to induce crack deflection and fibre pull-out mechanisms. However, in the rubber-toughened thermoplastic composites the matrix toughness is high and thus the interface requirements derived from the more brittle, thermoset matrices may no longer apply.

Based on the results of this study, some implications for fibre/matrix interface requirements may be identified separately for the initiation and propagation components of fracture. In the initiation stage of fracture, a strong fibre–matrix interface can enhance strengthening due to the glass fibres and thereby, as discussed in the previous section, provide positive fibre contributions to toughening. Furthermore, a strong fibre–matrix interface, in the presence of rubber particles, promotes craze energy dissipation at fibre–matrix interfaces, thereby enhancing toughness contribution from the fibre–matrix interfaces. On the other hand, a strong fibre–matrix interface can decrease the matrix craze contribution to toughness because of the stress shielding effect of the fibres. At the other extreme, too weak an interface would facilitate void initiation at the fibre–matrix interface and retard the initiation toughness. Thus it would appear that some optimum fibre–matrix interface strength is desirable for maximum initiation toughness. Too weak an interface would promote void formation at interfaces, whereas too strong an interface would preclude matrix contributions to toughening derived from crazing at added rubber particles.

As in the initiation stage, the propagation stage of fracture also appears to require some optimum interface strength. We note that, in this study, fibre pull-out rather than fibre fracture was largely observed. Further increases in interface strength will therefore increase energy dissipation by fibre pull-out. However, a strong interface can decrease the matrix craze zone in the crack wake by the stress shielding effect of the fibres, thereby decreasing the matrix contributions to the R curve. These trends are summarized in Table III. From the table it is clear that a stronger fibre–matrix interface enhances toughness contributions from the fibre–matrix interface and fibre itself, but tends to decrease toughness contributions from the matrix.

TABLE III Trends in toughness contributions from matrix, fibre and interface due to changes in interface strength

	Interface strength	Toughness contributions		
		From matrix	From interface	From fibre
Initiation toughness	Increase	Decrease	Increase	Increase
Propagation toughness (R curve)	Increase	Decrease	Increase	Increase

More detailed studies are required to determine the optimum interface strength requirements for this composite system.

4. Summary and conclusions

1. Glass-fibre additions increase the toughness of untoughened matrices, but decrease the toughness of the rubber-toughened materials at small fibre contents. Beyond about 10 wt % glass-fibre content, the toughness of all materials is increased.

2. The decrease in toughness is associated with the inhibition of crazing at rubber particles due to the glass fibres and the promotion of void formation at glass-fibre ends by the rubber particles.

3. An additional deformation and toughening mechanism was identified in the presence of glass, namely, craze formation at the glass fibre–matrix interfaces promoted by the rubber particles.

4. Glass fibres contribute to propagation toughness by fibre bridging of the matrix crack and by fibre pull-out, as well as by promoting crack deflection.

5. Some possible roles of the fibre–matrix interfaces in toughness are suggested. However, the optimum interface property requirements, in terms of whether a strong or a weak interface is desirable, were not conclusively identified.

Acknowledgements

This work was supported by the National Science Foundation under Grant MSM-8552720 and by a grant from the Monsanto Chemical Company, Springfield, Massachusetts. Helpful discussions with Dr Robert L. Kruse of Monsanto Chemical Company is also gratefully acknowledged. The authors also thank B. G. Cunningham of Monsanto Chemical Co. for assistance with TEM.

References

1. M. J. FOLKES, "Short Fiber Reinforced Thermoplastic Composites" (Research Studies Press, Chichester, 1982) p. 27.
2. D. SHORT and J. SUMMERSCALES, *Composites* **10** (1979) 215.
3. *Idem, ibid.* **11** (1980) 33.
4. J. LIAU, B. JANG, L. HWANG and R. WILCOX, in Proceedings of "ANTEC '88" (Society of Plastic Engineers, 1988) p. 1649.
5. R. S. BAILEY and M. G. BADER, in Proceedings of the 5th International Conference on Composite Materials, San Diego, 1985 (Metallurgical Society, 1985) p. 947.
6. B. L. PETERSON, R. N. PANGBORN and C. G. PANTANO, submitted to "ISTFA '89 Advanced Materials Symposium", International Symposium for Testing and Failure Analysis, Los Angeles, Nov. 1989.
7. J. M. SCOTT and D. C. PHILLIPS, *J. Mater. Sci.* **10** (1975) 551.
8. K. FRIEDRICH, in Proceedings of the 5th International Conference on Deformation, Yield and Fracture of Polymers, Cambridge, March 1982 (Plastic and Rubber Institute, London, 1982) p. 26.1.
9. W. V. TITOW and B. J. LANHAN, "Reinforced Thermoplastics" (Applied Science, London, 1975) p. 159.
10. A. J. KINLOCH, D. L. MAXWELL and R. J. YOUNG, *J. Mater. Sci.* **20** (1985) 4169.
11. H. RICHTER, *Kunststoffe* **67** (1977) 739 (in German).
12. C. B. BUCKNALL, "Toughened Plastics" (Applied Science, London, 1977) p. 1.
13. R. P. KAMBOUR, *Macromol. Rev.* **7** (1973) 1.
14. J. N. SULTAN and F. J. McGARRY, *Polym. Engng Sci.* **13** (1973) 29.
15. A. M. DONALD and E. J. KRAMER, *J. Mater. Sci.* **17** (1982) 1765.
16. A. S. ARGON and R. E. COHEN, in "Crazing in Polymers", Vol. II, Advances in Polymer Science Series, Vol. 91/92, edited by H. H. Kauch (Springer-Verlag, Berlin, 1990) p. 301.
17. A. M. DONALD and E. J. KRAMER, *J. Mater Sci.* **17** (1982) 1871.
18. F. HAAF, H. BREUER and J. STABENOW, *J. Macromol. Sci. Phys.* **B14** (1977) 387.
19. K. T. FABER and A. G. EVANS, *Acta. Metall.* **31** (1983) 565.
20. P. W. R. BEAUMONT, *Mater. Forum* **11** (1988) 332.
21. N. SATO, T. KURAUCHI, S. SATO and O. KAMIGAITO, *J. Comp. Mater.* **22** (1988) 850.
22. R. A. MENDELSON, *J. Polym. Sci. Polym. Phys. Edn* **23** (1985) 1975.
23. P. W. EARLY and S. J. BURNS, *Int. J. Fract.* **16** (1980) 397.
24. P. CHANG and J. A. DONOVAN, *J. Mater. Sci.* **24** (1989) 816.
25. D. BEAHAN, A. THOMAS and M. BEVIS, *ibid.* **11** (1976) 1207.
26. C. B. BUCKNALL, F. F. P. COTE and I. K. PARTRIDGE, *ibid.* **22** (1987) 1341.
27. C. C. CHAU and J. C. M. LI, *ibid.* **16** (1981) 1858.
28. N. WALKER, R. N. HAWARD and J. N. HAY, *ibid.* **14** (1979) 1085.
29. A. J. KINLOCH and R. J. YOUNG, "Fracture Behaviors of Polymers" (Applied Science, London, 1983) p. 137.
30. D. BROEK, "Elementary Engineering Fracture Mechanics" (Martinus Nijhoff, Boston, 1986) p. 232.
31. A. G. EVANS, Z. B. AHMAD, D. G. GILBERT and P. W. R. BEAUMONT, *Acta Metall.* **34** (1986) 79.
32. S. KUNZ-DOUGLASS, P. W. R. BEAUMONT and M. F. ASHBY, *J. Mater. Sci.* **15** (1980) 1109.
33. S. V. NAIR and M. L. SHIAO, "Crack Wake Dilatational Toughening in Rubber Toughened Polymers", to be published.
34. A. H. COTTRELL, *Proc. R. Soc., Lond.* **A282** (1964) 2.
35. G. A. COOPER and A. KELLY, *ASTM STP* **452** (1969) 90.
36. C. B. BUCKNALL, "Toughened Plastics" (Applied Science, London, 1977) p. 195.

Received 21 November 1990
and accepted 10 April 1991